Dalton Transactions

ROYAL SOCIETY OF CHEMISTRY

PAPER

View Article Online
View Journal | View Issue

Cite this: *Dalton Trans.*, 2025, **54**, 10433

Flux crystal growth, structure, and optical properties of non-centrosymmetric oxysulfides $Ln_3Ga_3Ge_2S_3O_{10}$ (Ln = La, Ce, Pr, Nd)†

Hong Yan,[a,b] Kotaro Fujii,[c,d] Yoshitaka Matsushita,[e] Masatomo Yashima,[c] Kazunari Yamaura[a,b] and Yoshihiro Tsujimoto *[a,b]

Single crystals of the non-centrosymmetric oxysulfides $Ln_3Ga_3Ge_2S_3O_{10}$ (Ln = La, Ce, Pr, Nd) in a hexagonal space group $P\bar{6}2c$ were grown by a flux crystal growth method using a eutectic $BaCl_2$–NaCl molten salt. Single-crystal X-ray diffraction analysis of them revealed that the Ga and Ge atoms were located on the 6*g* and 4*f* sites, which were tetrahedrally coordinated with two O and two S atoms, and four O atoms, respectively. In the structure, the GaS_2O_2 and GeO_4 tetrahedra form $^1_\infty[Ga_3S_3O_3]$ triangular tubes and Ge_2O_7 tetrahedral dimers aligned along the *c* axis, which are surrounded by LaS_2O_6 square prisms in the *ab* plane. Neutron powder diffraction studies on polycrystalline samples of $La_3Ga_3Ge_2S_3O_{10}$ and $Nd_3Ga_3Ge_2S_3O_{10}$ which were prepared by high-temperature solid state reactions supported the Ga/Ge cation order determined by the single-crystal structure analysis. UV-Vis-NIR absorption spectra revealed band gaps larger than 4.60 eV for $La_3Ga_3Ge_2S_3O_{10}$, $Pr_3Ga_3Ge_2S_3O_{10}$, and $Nd_3Ga_3Ge_2S_3O_{10}$, while $Ce_3Ga_3Ge_2S_3O_{10}$ was found to have a small band gap value of 3.51 eV because of the Ce-$4f^1$ electronic configuration.

Received 9th May 2025,
Accepted 4th June 2025

DOI: 10.1039/d5dt01100k

rsc.li/dalton

Introduction

Metal oxychalcogenides, in which oxide and chalcogenide ions coexist in one structure, have provided a playground for solid-state scientists to explore fascinating properties because of the large differences in their ionic radii, electronegativities, oxidation states, and polarizabilities.[1,2] One recent significant advantage of oxychalcogenide compounds is the design of nonlinear optical (NLO) materials.[3,4] Stabilizing metal-centered heteroleptic coordination environments containing both oxide and chalcogenide ligands offers a chance to significantly increase the optical band gaps and second harmonic generation (SHG) responses compared with chalcogenides, because of the presence of O 2p orbitals in the valence band maximum and acentric polyhedral units with polar atomic displacement. Since the discovery of the first phase-matchable oxyselenide $BaGeOSe_2$ and oxysulfide $SrZn_2S_2O$ with strong SHG intensities,[5,6] a number of new oxychalcogenides have been reported to show good balanced properties with high SHG responses, high laser damage thresholds, and wide optical band gaps.[3,7] While most of the reported NLO oxychalcogenide compounds were focused on applications in the infrared region because of their relatively small band gap values (<4 eV),[7] a new oxysulfide $La_3Ga_3Ge_2S_3O_{10}$ consisting of $(Ga/Ge)O_4$ and $(Ga/Ge)S_2O_2$ tetrahedra exhibited promising properties for applications in the UV regions (Fig. 1): the exceptionally large band gap value (4.70 eV), short cutoff edge (250 nm), and strong SHG response twice that of the KH_2PO_4 benchmark compound.[8] The fundamental origin of the large bandgap and strong SHG response can be attributed to the lack of an all-sulfide coordination environment and the presence of a heteroleptic coordination environment,[9,10] as in $[Ba_2F_2][Ge_2O_3S_2]$ (1.4 × $AgGaS_2$),[11] $Nd_3Ga_3Ge_2S_3O_{10}$ (1.7 × KDP, 0.8 × $AgGaS_2$),[12] and $La_3Ga_3Si_2S_3O_{10}$ (1.7 × KDP, 0.3 × $AgGaS_2$).[13]

Single-crystal X-ray diffraction (SCXRD) analyses of $La_3Ga_3Ge_2S_3O_{10}$, $La_3Ga_3Si_2S_3O_{10}$, and $Nd_3Ga_3Ge_2S_3O_{10}$ have demonstrated that they are isostructural and adopt a hexagonal unit cell in the space group $P\bar{6}2c$.[8,12,13] However, they exhibited different atomic distribution patterns, as described below. In the

[a]*Research Center for Materials Nanoarchitechtonics (MANA), National Institute for Materials Science (NIMS), 1-1 Namiki, Tsukuba, Ibaraki 305-0044, Japan. E-mail: TSUJIMOTO.Yoshihiro@nims.go.jp*
[b]*Graduate School of Chemical Sciences and Engineering, Hokkaido University, North 10 West 8, Kita-ku, Sapporo, Hokkaido 060-0810, Japan*
[c]*Department of Chemistry, School of Science, Institute of Science Tokyo, 2-12-1-W4-17, Ookayama Meguro-ku, Tokyo, 152-8551, Japan*
[d]*Faculty of Bioscience and Applied Chemistry, Department of Chemical Science and Technology, Hosei University, 3-5-4 Kajino-cho, Koganei, Tokyo 184-8584, Japan*
[e]*Materials Analysis Station, NIMS, 1-2-1 Sengen, Tsukuba, Ibaraki 305-0047, Japan*

† Electronic supplementary information (ESI) available. CCDC 2449159, 2449160, 2449238 and 2449239. For ESI and crystallographic data in CIF or other electronic format see DOI: https://doi.org/10.1039/d5dt01100k

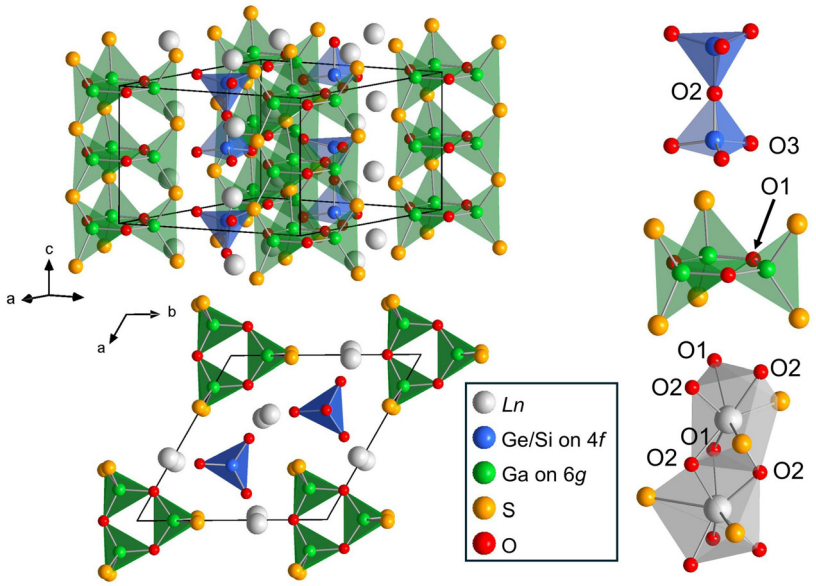

Fig. 1 Side and top views of the crystal structure of $Ln_3Ga_3Ge_2S_3O_{10}$ (Ln = La, Ce, Pr, Nd), which possesses one-dimensional chains of LnS_2O_6 square antiprisms, and isolated dimers and triangular tubes composed of $M1O_4$ tetrahedra and $M2S_2O_2$ tetrahedra, respectively.

latter two phases, the Ga and Ge/Si atoms were located on Wyckoff positions 6*g* and 4*f*, respectively, to take the GaS_2O_4 and $(Ge/Si)O_4$ tetrahedral geometries (Fig. 1). These tetrahedra formed $^1_\infty[Ga_3S_3O_3]$ triangular tubes and $(Ge/Si)_2O_7$ tetrahedral dimers, which were separated by $(La/Nd)S_2O_6$ square antiprisms in the *ab* plane. In contrast, $La_3Ga_3Ge_2S_3O_{10}$ exhibited a random distribution of Ga and Ge over the 6*g* and 4*f* sites at an atomic ratio of 3 : 2. It is reasonable for Si ions to adopt an all-oxygen homoleptic coordination geometry because they rarely form heteroleptic coordination polyhedra, while the difference in cation ordering patterns in $La_3Ga_3Ge_2S_3O_{10}$ and $Nd_3Ga_3Ge_2S_3O_{10}$ is non-trivial. In previous studies, the bond-valence-sum (BVS) values for Ga/Ge on 6*g* and 4*f* were estimated to be 3.04 and 3.92, respectively. This implied a Ga/Ge ordered state as in the Nd analog, although structural refinements based on the cation-ordered model were unstable. In oxides containing both Ga and Ge atoms, the identification of the distribution of these cations by XRD analysis is of major concern because of their similar X-ray scattering factors.[14–16]

In this study, we reexamined the Ga/Ge cation disordered state of $La_3Ga_3Ge_2S_3O_{10}$ and newly synthesized a series of $Ln_3Ga_3Ge_2S_3O_{10}$ (Ln = La, Ce, Pr, Nd) by both molten chloride flux methods and conventional solid-state reactions. Neutron powder diffraction (NPD), in addition to SCXRD, was employed to characterize the crystal structure, especially the Ga/Ge cation ordered pattern.

Experimental section

Reagents

La_2S_3 (Kojundo Chemical Laboratory, 3 N), La_2O_3 (Rare Metallic, 4 N), CeO_2 (Rare Metallic, 4 N), Pr_6O_{11} (Rare Metallic, 3 N), Nd_2O_3 (Rare Metallic, 3 N), Ga_2O_3 (Rare Metallic, 3 N), GeO_2 (Rare Metallic, 4 N), Ge (Kojundo Chemical Laboratory, 4 N), S (Kojundo Chemical Laboratory, 4 N), $BaCl_2$ (Rare Metallic, 3 N), and NaCl (Rare Metallic, 4 N) powders were used as received. $BaCl_2$ and NaCl were heated overnight at 370 °C prior to use. La_2O_3 was preheated at 1000 °C in air prior to use. All raw materials were stored in an argon-filled glovebox (moisture and oxygen levels less than 0.1 ppm), and all manipulations before starting the reaction were carried out in a glovebox or under vacuum.

Crystal growth and elemental analysis

Single crystals of $Ln_3Ga_3Ge_2S_3O_{10}$ (Ln = La, Ce, Pr, Nd) were obtained by the flux growth method using a $BaCl_2$–NaCl eutectic molten salt. For Ln = La, La_2S_3 (0.5 mmol), Ga_2O_3 (0.5 mmol), and GeO_2 (0.5 mmol) were combined according to the literature.[8] For Ln = Ce and Pr, CeO_2 (0.6 mmol)/Pr_6O_{11} (0.1 mmol), Ga_2O_3 (0.3 mmol), Ge (0.4 mmol), and S (0.6 mmol) were combined. For Ln = Nd, Nd_2O_3 (0.3 mmol), Ga_2O_3 (0.3 mmol), Ge (0.3 mmol), S (0.6 mmol) and GeO_2 (0.1 mmol) were combined. Each set of starting materials was loaded in an alumina crucible with $BaCl_2$ (2.7 mmol) and NaCl (4.0 mmol). The crucibles were flame-sealed in fused silica tubes under a vacuum of 1 Pa, heated in a muffle furnace to 850 °C at 5 °C min^{-1}, held at this temperature for 24 h, cooled to 550 °C at 0.08 °C min^{-1}, and finally cooled naturally to room temperature. The products were then washed with sonicated water and extracted from the flux. Transparent rod-shaped crystals of the title compounds were collected by vacuum filtration with approximately yields of 65% for La, 10% for Ce, 30% for Pr, and 60% for Nd based on lanthanide (Fig. 2). Elemental analysis of single crystals of

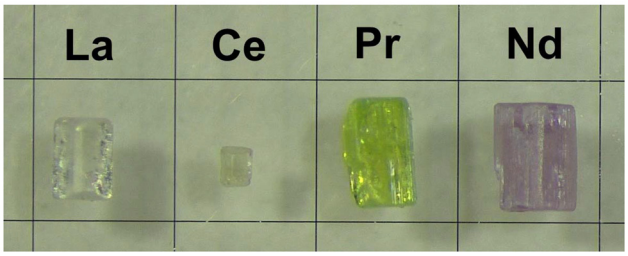

Fig. 2 Photographs of single crystals of $Ln_3Ga_3Ge_2S_3O_{10}$ (Ln = La, Ce, Pr, Nd) on a 1 mm-grid glass plate.

$Ln_3Ga_3Ge_2S_3O_{10}$ was performed using a scanning electron microscope (SEM, HITACHI, S-43000) equipped with an energy dispersive X-ray (EDX) spectrometer. The accelerating voltage was set to 15 keV. EDX analysis indicated a Ln : Ga : Ge : S atomic ratio of approximately 3 : 3 : 2 : 3, which was in good agreement with the chemical composition determined by single-crystal structure analysis.

Solid state reaction

Polycrystalline powder samples of $Ln_3Ga_3Ge_2S_3O_{10}$ (Ln = La–Nd) were synthesized by conventional solid-state reactions. The Ln = La, Pr, and Nd phases were synthesized from a stoichiometric mixture of La_2O_3 (0.3 mmol), Ga_2O_3 (0.3 mmol), GeO_2 (0.1 mmol), Ge (0.3 mmol), and S (0.6 mmol) for Ln = La, Pr_6O_{11} (0.1 mmol), Ga_2O_3 (0.3 mmol), Ge (0.4 mmol) and S (0.6 mmol) for Ln = Pr, Nd_2O_3 (0.3 mmol), Ga_2O_3 (0.3 mmol), GeO_2 (0.1 mmol), Ge (0.3 mmol), and S (0.6 mmol) for Ln = Nd. The Ln = Ce phase was synthesized using a mixture of CeO_2 (0.6 mmol), Ga_2O_3 (0.3 mmol), Ge (0.4 mmol), and S (0.6 mmol), which contains 0.1 mmol excess of oxygen compared with the stoichiometry of $Ce_3Ga_3Ge_2S_3O_{10}$. Each set of starting materials was ground with an agate mortar and pestle, pressed into a pellet, sealed in a silica tube under a vacuum of 1 Pa, and heated in a muffle furnace at 1000 °C for 24 h. For neutron powder diffraction studies, scaled-up syntheses (approximately 10 times the amount) of polycrystalline powder samples of $La_3Ga_3Ge_2S_3O_{10}$ and $Nd_3Ga_3Ge_2S_3O_{10}$ were performed using a similar synthesis procedure.[8,12]

Single crystal structure determination

X-ray intensity data of single crystals of $Ln_3Ga_3Ge_2S_3O_{10}$ (Ln = La–Nd) were collected using a Rigaku XtaLAB mini II diffractometer (Mo Kα radiation). Data collection covered more than 96% of the reciprocal space to $2\theta_{max} \sim 60°$ with R_{int} = 4.17% for La, 3.42% for Ce, 3.19% for Pr, and 3.31% for Nd after absorption correction. The crystal structure was solved using a dual-space algorithm method (SHELXT)[17] and refined using a full-matrix least-squares method with SHELXL[18] using an Olex2[19] graphical user interface.

Powder XRD and UV-Vis-NIR

Powder XRD patterns were collected on a Rigaku MiniFlex-600 diffractometer (Cu Kα radiation) from the 2θ range of 5–70° with a step of 0.02° at room temperature. The UV-vis–NIR reflectance spectra were collected using a Shimadzu UV- 2600 UV-Vis-NIR spectrometer (used in the diffuse reflectance mode) equipped with an integrating sphere in the range of 220–1200 nm. Deuterium and halogen lamps were used as sources of UV and visible-NIR light, respectively. The recorded reflectance spectra were converted into the absorption data *via* the Kubelka–Munk function.

Powder neutron diffraction

Time-of-flight neutron powder diffraction (NPD) measurements were conducted at room temperature using an iMATERIA[20] installed at J-PARC MLF BL20 in Japan. $La_3Ga_3Ge_2S_3O_{10}$ (2.44 g) and $Nd_3Ga_3Ge_2S_3O_{10}$ (2.57 g) were independently loaded into a vanadium can with 5.8 mm inner diameter, and the diffraction data were collected using a back-scattering detector bank. The NPD data were analyzed by Rietveld refinement using the Z-code program.[21]

Results and discussion

Structure determination using single-crystal X-ray diffraction data

Typical dimensions of single crystals of $Ln_3Ga_3Ge_2S_3O_{10}$ (Ln = La–Nd) were ranged from 0.1 × 0.1 × 0.2 to 0.5 × 0.5 × 0.8 mm^3, indicating that these crystals grew preferentially along the *c*-axis. Single crystals of $La_3Ga_3Ge_2S_3O_{10}$ and $Nd_3Ga_3Ge_2S_3O_{10}$ were colorless and pale purple, respectively, as previously reported (Fig. 2). $Ce_3Ga_3Ge_2S_3O_{10}$ and $Pr_3Ga_3Ge_2S_3O_{10}$ were colorless and lime-green, respectively. The colors of $Pr_3Ga_3Ge_2S_3O_{10}$ and $Nd_3Ga_3Ge_2S_3O_{10}$ are characteristic of f–f transitions in Pr^{3+} and Nd^{3+}. These single crystals are stable in air and water insoluble. Single-crystal structure analysis of $Ln_3Ga_3Ge_2S_3O_{10}$ (Ln = La–Nd) was performed at room temperature. As reported previously, the Ln = La phase adopts the hexagonal space group $P\bar{6}2c$ (no. 190) with lattice parameters of a = 10.1701(4) Å and c = 7.5198(3) Å.[8] Additionally, the structure refinement based on the cation ordered model that Ga and Ge atom occupied 6*g* and 4*f* sites, respectively, smoothly converged in contrast to our previous report. The Ln = Ce–Nd analogs were also found to adopt the same space group with lattice parameters, which were proportional to the ionic radius of Ln^{3+} ions (Fig. 3). The structure refinements indicated the Ga/Ge ordering, as reported previously for $Nd_3Ga_3Ge_2S_3O_{10}$.[12] The details of the final refined structure for all the phases are listed in Table 1. The atomic coordinates and isotropic thermal displacement parameters are listed in Table 2 and the anisotropic displacement parameters are listed in Table S1.† Selected interatomic distances and angles are listed in Table S2.† The metal–ligand bond distances in GeO_4 and GaS_2O_2 tetrahedra in all phases are very close to the sum of their ionic radii ($r_{Ge^{4+}}$ = 0.39 Å, $r_{Ga^{3+}}$ = 0.47 Å, $r_{O^{2-}}$ = 1.4 Å, $r_{S^{2-}}$ = 1.84 Å).[22] In contrast, in the LnS_2O_6 tetrahedron, the Ln–O/Ln–S bond distances are broad compared to the sum of their ionic radii, but their average bond distances are in good agreement

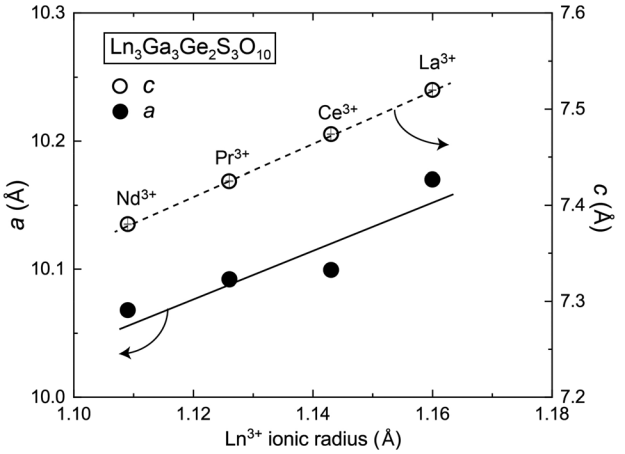

Fig. 3 The *a*-axis and *c*-axis lengths plotted as a function of the ionic radius of Ln^{3+}.

with the sum of their ionic radii. Bond valence sum (BVS) calculations[23] were carried out for all the atoms, as shown in Table 3. The BVS values of Ln (= La, Ce, Pr, Nd), Ga, and Ge atoms were consistent with the nominal oxidation number expected from the chemical composition.

X-ray powder diffraction

Fig. 4 shows the room-temperature X-ray powder diffraction patterns of polycrystalline $Ln_3Ga_3Ge_2S_3O_{10}$ (Ln = La–Nd) samples synthesized by conventional high-temperature solid-state reactions. These compounds were obtained in nearly a single phase. All of these XRD patterns could be readily indexed to the hexagonal cell in the space group $P\bar{6}2c$, except for a few minor peaks that could be assigned to GeO_2. Similar to the single-crystal structure analysis, the lattice constants of the polycrystalline samples also varied with the ionic radius of Ln^{3+} (Fig. S1†).

Structure determination using neutron powder diffraction data

To investigate the Ga and Ge atom distribution in $La_3Ga_3Ge_2S_3O_{10}$, neutron powder diffraction experiments were performed on $La_3Ga_3Ge_2S_3O_{10}$ at room temperature, together with $Nd_3Ga_3Ge_2S_3O_{10}$, for comparison. Fig. 5 shows the results of Rietveld refinements of these two oxysulfides. For both $La_3Ga_3Ge_2S_3O_{10}$ and $Nd_3Ga_3Ge_2S_3O_{10}$, the profile fitting to the Ga/Ge ordered model smoothly converged well with reliable factors, R_{wp} = 5.40, R_p = 4.24, R_B = 2.58 for La and R_{wp} = 8.24, R_p = 5.79, R_B = 5.97 for Nd (Fig. 5). To examine the possibility of Ga/Ge atoms being disordered, structure refinement was performed under the assumption that Ga and Ge atoms are disordered at the 6*g* and 4*f* sites. The results showed that 6*g* and 4*f* sites were more than 99% occupied by Ga and Ge atoms, respectively, within statistical errors. Thus, we conclude that the Ga and Ge atoms in the polycrystalline samples are ordered like the single crystals. Tables S3 and Table 3 summarize the final obtained crystallographic data including isotropic displacement parameters for all atoms. The occupancy factors of Ga on 6*g* and Ge on 4*f* were fixed at unity in the final refinement.

Ga/Ge cation ordering and size effect of Ln^{3+} on the lattices

The present structure refinements against the SCXRD and NPD data of $La_3Ga_3Ge_2S_3O_{10}$ revealed the Ga/Ge cation order, which differed from the Ga/Ge disorder characterized in the previous study.[8] One possible reason for the cation disordering can be ascribed to a technical problem in the structure refinements. We reviewed the previous SCXRD data from the beginning and found that the cation ordered state was also stabil-

Table 1 Results of structure refinement of $Ln_3Ga_3Ge_2S_3O_{10}$ (Ln = La, Ce, Pr, Nd) using single-crystal XRD data

Formula	$La_3Ga_3Ge_2S_3O_{10}$	$Ce_3Ga_3Ge_2S_3O_{10}$	$Pr_3Ga_3Ge_2S_3O_{10}$	$Nd_3Ga_3Ge_2S_3O_{10}$
Formula weight	1027.25	1030.88	1033.25	1043.24
T (K)	297	297	293	294
Crystal system	Hexagonal	Hexagonal	Hexagonal	Hexagonal
Space group	$P\bar{6}2c$	$P\bar{6}2c$	$P\bar{6}2c$	$P\bar{6}2c$
a (Å)	10.1701(4)	10.0993(4)	10.0921(7)	10.0682(5)
c (Å)	7.5198(3)	7.4738(4)	7.4251(5)	7.3802(5)
α (°)	90	90	90	90
β (°)	90	90	90	90
γ (°)	120	120	120	120
V (Å^3)	673.58(6)	660.17(6)	654.93(9)	647.89(8)
Z	2	2	2	2
ρ_{calc} (g cm^{-3})	5.065	5.186	5.240	5.348
μ (mm^{-1})	20.096	21.201	22.042	23.023
F_{000}	912	918	924	930
θ (°)	3.534–30.53	2.329–30.64	3.5840–30.38	2.336–30.607
R_{int} (%)	4.17	3.42	3.19	3.31
No. of reflections (collected/unique)	9330/734	9529/723	2246/467	2524/658
Goodness of fit on F^2	1.061	1.083	0.977	1.041
R_1, wR_2 [$I > 2\sigma(I)$]	0.0109, 0.0251	0.0109/0.0208	0.0128/0.0234	0.0192/0.0378
R_1, wR_2 (all data)	0.0114, 0.0252	0.0126/0.0210	0.0136/0.0236	0.0216/0.0386
Diff peak, hole (e Å^{-3})	0.433, −0.387	0.454, −0.494	0.373, −0.330	0.712, −0.644
Flack parameter	−0.002(13)	0.001(12)	−0.03(3)	−0.05(3)

Table 2 Crystallographic and refinement data obtained from single-crystal structure analysis of $Ln_3Ga_3Ge_2S_3O_{10}$ (Ln = La, Ce, Pr, Nd)

Atom	Site	x	y	z	Occupancy	U_{iso}/ Å^2
$La_3Ga_3Ge_2S_3O_{10}$						
La	6*h*	0.35751(3)	0.38034(3)	1/4	1	0.00771(8)
Ge	4*f*	2/3	1/3	0.51367(7)	1	0.00446(13)[a]
Ga	6*g*	0	0.18935(5)	0	1	0.00652(12)[a]
S	6*h*	0.01248(14)	0.32093(14)	1/4	1	0.0106(2)
O1	6*g*	0.1757(3)	0.1757(2)	0	1	0.0089(7)
O2	12*i*	0.5052(3)	0.3439(3)	0.4667(3)	1	0.0111(5)
O3	2*c*	2/3	1/3	3/4	1	0.033(2)
$Ce_3Ga_3Ge_2S_3O_{10}$						
Ce	6*h*	0.35730(3)	0.38047(3)	1/4	1	0.00888(7)
Ge	4*f*	2/3	1/3	0.51309(7)	1	0.00542(13)
Ga	6*g*	0	0.19034(6)	0	1	0.00761(11)
S	6*h*	0.01396(15)	0.32373(15)	1/4	1	0.0120(3)
O1	6*g*	0.1770(3)	0.1770(3)	0	1	0.0111(7)
O2	12*i*	0.5038(3)	0.3439(3)	0.4663(3)	1	0.0115(5)
O3	2*c*	2/3	1/3	3/4	1	0.032(2)
$Pr_3Ga_3Ge_2S_3O_{10}$						
Pr	6*h*	0.35754(5)	0.38139(6)	1/4	1	0.00797(13)
Ge	4*f*	2/3	1/3	0.51145(11)	1	0.0039(2)
Ga	6*g*	0	0.19057(10)	0	1	0.0070(2)
S	6*h*	0.01632(2)	0.3260(2)	1/4	1	0.0118(5)
O1	6*g*	0.1764(6)	0.1764(6)	0	1	0.0135(15)
O2	12*i*	0.5033(4)	0.3433(4)	0.4658(5)	1	0.0106(9)
O3	2*c*	2/3	1/3	1/4	1	0.036(4)
$Nd_3Ga_3Ge_2S_3O_{10}$						
Nd	6*h*	0.35688(5)	0.38212(6)	1/4	1	0.00923(14)
Ge	4*f*	2/3	1/3	0.51014(13)	1	0.0056(2)
Ga	6*g*	0	0.19121(11)	0	1	0.0076(2)
S	6*h*	0.0183(3)	0.3287(3)	1/4	1	0.0121(5)
O1	6*g*	0.1778(6)	0.1778(6)	0	1	0.0123(14)
O2	12*i*	0.5029(5)	0.3435(5)	0.4643(6)	1	0.0114(9)
O3	2*c*	2/3	1/3	1/4	1	0.036(4)

Table 3 The values of bond-valence-sum calculations for Ln, Ge, and Ga sites obtained from the single crystal structure analysis

Formula	Ln at 6*h*	Ga at 6*g*	Ge at 4*f*
$La_3Ga_3Ge_2S_3O_{10}$	2.81	3.03	3.91
$Ce_3Ga_3Ge_2S_3O_{10}$	2.83	2.95	4.03
$Pr_3Ga_3Ge_2S_3O_{10}$	2.92	2.98	4.05
$Nd_3Ga_3Ge_2S_3O_{10}$	2.81	2.98	4.04

ized. Perhaps, due to similar X-ray scattering factors of Ga and Ge atoms, the previous refinements fell into a local minimum that stabilizes the cation disordered state.

As shown in Fig. 3, the lattice parameters change linearly with the ionic radius of the Ln^{3+}. On the other hand, the distortion index[24] (D) around the metal centers, which was calculated using the metal–anion bond distances determined from the SCXRD data, exhibits unusual behaviors against the size of Ln^{3+} (Table S4†). The D values for the Ge-centered tetrahedra in Ln = La are 0.00911, which are remarkably larger than those for the corresponding tetrahedra in the other Ln ions by 15–31%, while the D values for the Ln- and Ga-centered polyhedra remained similar regardless of the Ln species. This can be rationalized by considering the volume of LnO_6S_2 square antiprisms, which form three-member rings *via* common S atoms in the *ab* plane and surround the Ga/Ge-centered tetrahedra. The GeO_4 tetrahedron may be too small to fit into a framework consisting of LaS_2O_6, which has the largest volume compared to other Ln-centered polyhedra. We attempted to synthesize other members with Ln^{3+} smaller than Nd^{3+}, but it was not successful.

Optical properties and bandgap

Fig. 6a shows the UV-Vis–NIR diffuse reflectance of $Ln_3Ga_3Ge_2S_3O_{10}$ (Ln = La–Nd). The spectra of Ln = Pr and Nd exhibited a UV cutoff edge close to 250 nm, as seen for $La_3Ga_3Ge_2S_3O_{10}$, which can be attributed to an optical transition from the valence band maximum composed of Ln-5d and Ga-4s, 4p orbitals to the conduction band minimum composed of O-2p and S-3p orbitals.[8,12] A series of complex optical bands in a broad range of wavelengths result from the f–f transitions characteristic of the localized 4f orbitals of Ln ions. In contrast, the Ln = Ce phase exhibited stepwise absorption below 430 nm, followed by a cutoff edge at 340 nm. This characteristic absorption is due to the presence of the Ce-4f ground state between the VBM and CBM: optical transitions from the Ce-4f ground state to the lowest and second lowest Ce-4d states occur. Fig. 6b shows the absorption spectra converted from the diffuse reflectance spectra using the Kubelka–

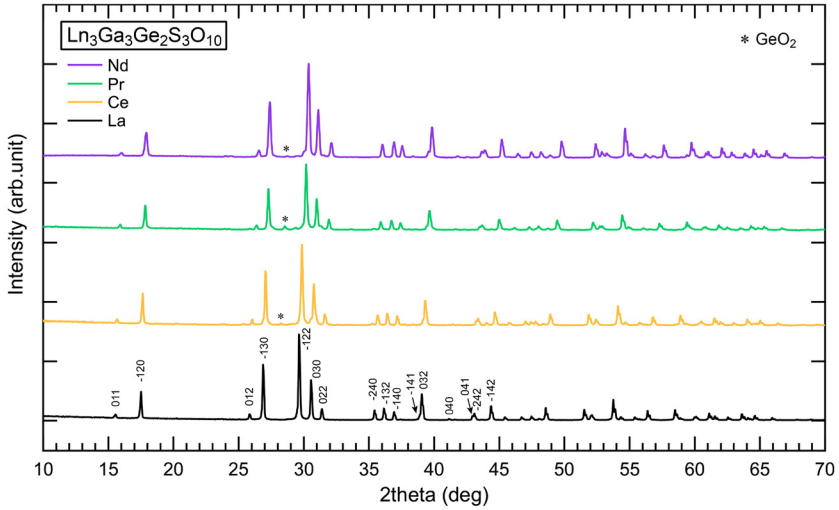

Fig. 4 Room-temperature X-ray powder diffraction patterns of $Ln_3Ga_3Ge_2S_3O_{10}$ (Ln = La, Ce, Pr, Nd) polycrystalline samples obtained *via* high-temperature solid-state reactions. All phases can be assigned to a hexagonal cell in the space group $P\bar{6}2c$.

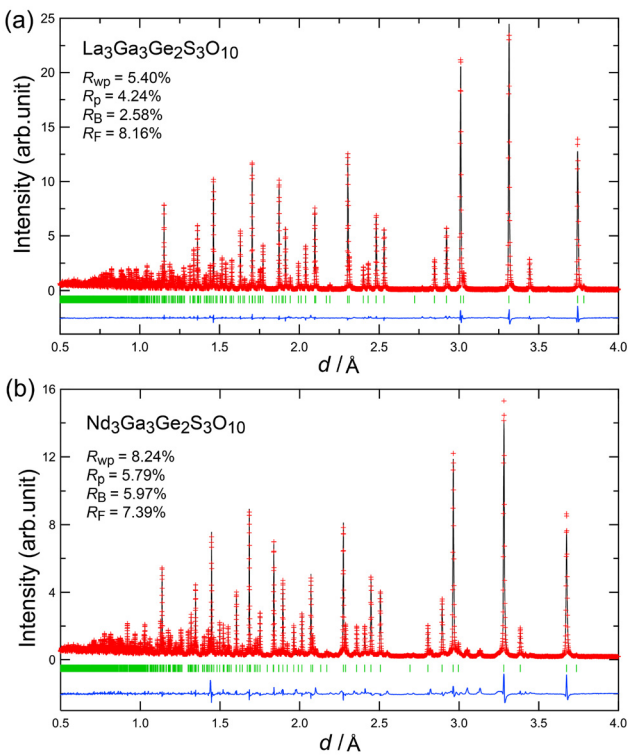

Fig. 5 Neutron powder diffraction patterns collected from (a) $La_3Ga_3Ge_2S_3O_{10}$ and (b) $Nd_3Ga_3Ge_2S_3O_{10}$ at room temperature. Rietveld refinements were performed on the basis of the structural models determined by single crystal structure analysis.

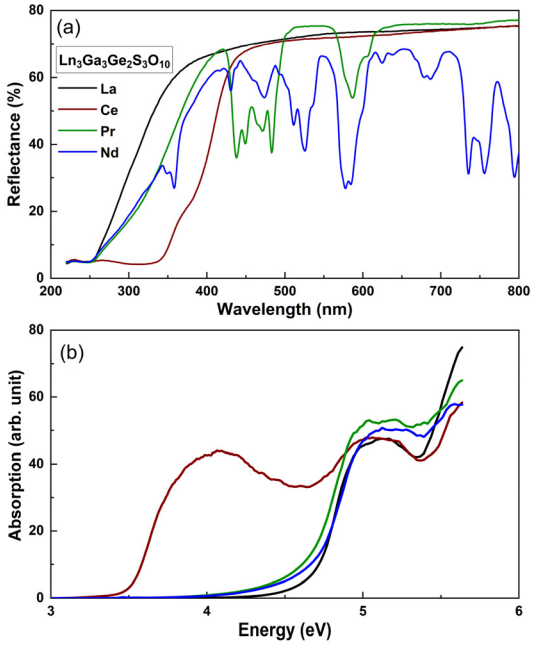

Fig. 6 (a) UV-Vis–NIR diffuse reflectance and (b) absorption spectra of $Ln_3Ga_3Ge_2S_3O_{10}$ (Ln = La, Ce, Pr, Nd). The bandgaps were estimated to be 4.70, 3.51, 4.60, and 4.64 eV, respectively.

Munk function. The optical band gaps of Ln = La, Ce, Pr, and Nd estimated by the extrapolation method were 4.70, 3.51, 4.60, and 4.64 eV, respectively. Similar band gap values for Ln = La, Pr, and Nd are consistent with the similar Ln 5d energy levels.[25]

SHG measurements

The powder SHG intensities of $Ln_3Ga_3Ge_2S_3O_{10}$ (Ln = Ce, Pr) were measured using the Kurtz–Perry method at λ = 1064 nm, with polycrystalline KDP as a reference compound. The SHG signals are plotted as a function of particle size in Fig. 7. The SHG intensities of both phases increased with increasing particle size in the size region smaller than 150 μm, and were almost saturated in the larger particle size region. These behaviors indicate that they are type-I phase-matchable like

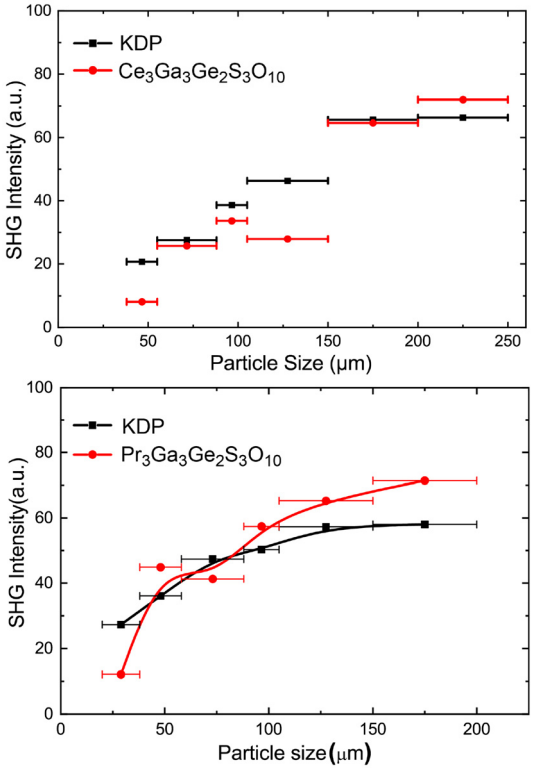

Fig. 7 Plots of SHG intensity *vs.* particle size at 1064 nm for $Ln_3Ga_3Ge_2S_3O_{10}$ (Ln = Ce, Pr) and the reference compound KH_2PO_4 (KDP). Solid lines are drawn as guides to the eyes.

$La_3Ga_3Ge_2S_3O_{10}$ and $Nd_3Ga_3Ge_2S_3O_{10}$.[8,12] The SHG intensities of Ln = Ce and Pr are comparable to that of KDP at the largest particle sizes measured, but somewhat smaller than those of the La and Nd analogs (~2 × KDP). These high SHG intensities are consistent with a previous theoretical conclusion that the Ga/Ge-centered tetrahedra forming non-centrosymmetric sublattices are mainly responsible for the SHG response of $La_3Ga_3Ge_2S_3O_{10}$.[8,26,27]

Conclusions

Although a Ga/Ge disordered state was previously suggested for single crystals of $La_3Ga_3Ge_2S_3O_{10}$, re-investigation by single-crystal XRD and neutron diffraction experiments performed in this study showed that $La_3Ga_3Ge_2S_3O_{10}$ has a Ga/Ge ordered state. Similar cation-ordered arrangements were observed for other lanthanide analogues. UV-Vis-NIR absorption spectra revealed band gaps larger than 4.60 eV for $La_3Ga_3Ge_2S_3O_{10}$, $Pr_3Ga_3Ge_2S_3O_{10}$, and $Nd_3Ga_3Ge_2S_3O_{10}$, except for $Ce_3Ga_3Ge_2S_3O_{10}$ with a small band gap value of 3.51 eV because of Ce-$4f^1$ electronic configuration.

Conflicts of interest

The authors declare no competing financial interests.

Data availability

The data supporting this article have been included as part of ESI. X-ray crystallographic files for the structure have been deposited in Cambridge Crystallographic Data Centre (CCDC) with no. of 2449159, 2449160, 2449238, and 2449239.†

Acknowledgements

This study was supported by World Premier International Research Center Initiative (WPI), the Japan Society for the Promotion of Science (JSPS) KAKENHI (grant no. 25K01507, 25K01657, 25H01652), Bilateral Program (No. JPJSBP120237714), and Core-to-Core Program (JPJSCCA20200004). Y. T. acknowledges the grant from the Murata Science Foundation. We also acknowledge Dr Ishigaki for his assistance in the NPD experiments with iMATERIA with the approval of J-PARC (Proposal No. 2023PM2001, 2024PM2001, 2025PM2002) and Prof. Z. Yang and Prof. S. Pan from Xinjiang Technical Institute of Physics and Chemistry, CAS for the SHG measurements.

References

1 H. Kageyama, K. Hayashi, K. Maeda, J. P. Attfield, Z. Hiroi, J. M. Rondinelli and K. R. Poeppelmeier, *Nat. Commun.*, 2018, **9**, 772.
2 M. Orr, G. R. Hebberd, E. E. McCabe and R. T. Macaluso, *ACS Omega*, 2022, **7**, 8209–8218.
3 J. Huang, S. Shu and G.-M. Cai, *Cryst. Growth Des.*, 2022, **22**, 1500–1514.
4 Y. Zhang, H. Wu, Z. Hu and H. Yu, *Chem. – Eur. J.*, 2023, **29**, e202203597.
5 B. W. Liu, X. M. Jiang, G. E. Wang, H. Y. Zeng, M. J. Zhang, S. F. Li, W. H. Guo and G. C. Guo, *Chem. Mater.*, 2015, **27**, 8189–8192.
6 Y. Tsujimoto, C. Juillerat, W. Zhang, K. Fujii, M. Yashima, P. S. Halasyamani and H.-C. zur Loye, *Chem. Mater.*, 2018, **30**, 6486–6493.
7 J. jing Xu and K. Wu, *Coord. Chem. Rev.*, 2023, **486**, 215139.
8 H. Yan, Y. Matsushita, K. Yamaura and Y. Tsujimoto, *Angew. Chem., Int. Ed.*, 2021, **60**, 26561–26565.
9 B. Zhang, G. Shi, Z. Yang, F. Zhang and S. Pan, *Angew. Chem., Int. Ed.*, 2017, **56**, 3916–3919.
10 G. Shi, Y. Wang, F. Zhang, B. Zhang, Z. Yang, X. Hou, S. Pan and K. R. Poeppelmeier, *J. Am. Chem. Soc.*, 2017, **139**, 10645–10648.
11 H. Liu, Z. Song, H. Wu, Z. Hu, J. Wang, Y. Wu and H. Yu, *ACS Mater. Lett.*, 2022, **4**, 1593–1598.
12 M. Y. Ran, S. H. Zhou, W. B. Wei, B. X. Li, X. T. Wu, H. Lin and Q. L. Zhu, *Small*, 2023, **19**, 2300248.
13 M. S. Zhang, S. M. Pei, X. M. Jiang, B. W. Liu and G. C. Guo, *ACS Mater. Lett.*, 2024, **3**, 312–318.

14 A. P. Dudka and B. V. Mill', *Crystallogr. Rep.*, 2013, **58**, 594–603.
15 L. A. Gorelova, V. A. Yukhno, M. G. Krzhizhanovskaya and O. S. Vereshchagin, *J. Solid State Chem.*, 2024, **329**, 124429.
16 H. Bazzaoui, C. Genevois, D. Massiot, V. Sarou-Kanian, E. Veron, S. Chenu, P. Beran, M. J. Pitcher and M. Allix, *Inorg. Chem.*, 2022, **61**, 9339–9351.
17 G. M. Sheldrick, *Acta Crystallogr., Sect. A:Found. Adv.*, 2015, **71**, 3–8.
18 G. M. Sheldrick, *Acta Crystallogr., Sect. C:Struct. Chem.*, 2015, **71**, 3–8.
19 O. V. Dolomanov, A. J. Blake, N. R. Champness and M. Schröder, *J. Appl. Crystallogr.*, 2003, **36**, 1283–1284.
20 T. Ishigaki, A. Hoshikawa, M. Yonemura, T. Morishima, T. Kamiyama, R. Oishi, K. Aizawa, T. Sakuma, Y. Tomota, M. Arai, M. Hayashi, K. Ebata, Y. Takano, K. Komatsuzaki, H. Asano, Y. Takano and T. Kasao, *Nucl. Instrum. Methods Phys. Res., Sect. A*, 2009, **600**, 189–191.
21 R. Oishi, M. Yonemura, Y. Nishimaki, S. Torii, A. Hoshikawa, T. Ishigaki, T. Morishima, K. Mori and T. Kamiyama, *Methods Phys. Res., Sect. A*, 2009, **600**, 94–96.
22 R. D. Shannon, *Acta Crystallogr., Sect. A*, 1976, **32**, 751–767.
23 N. E. Brese and M. O'Keeffe, *Acta Crystallogr., Sect. B:Struct. Sci.*, 1991, **47**, 192–197.
24 W. H. Baur, *Acta Crystallogr., Sect. B*, 1974, **30**, 1195–1215.
25 Y. Shimizu and K. Ueda, *J. Lumin.*, 2015, **168**, 14–19.
26 B.-H. Lei, S. Pan, Z. Yang, C. Cao and D. J. Singh, *Phys. Rev. Lett.*, 2020, **125**, 187402.
27 Z. Yang and S. Pan, *Chin. Sci. Bull.*, 2024, **69**, 4197–4208.